

# Orbital quantization in the high magnetic field state of a charge-density-wave system

D. Andres<sup>1</sup>, M. V. Kartsovnik<sup>1</sup>, P. D. Grigoriev<sup>2</sup>, W. Biberacher<sup>1</sup> and H. Müller<sup>3</sup>

<sup>1</sup> *Walther-Meißner-Institut, Bayerische Akademie der Wissenschaften,  
Walther-Meißner-Str. 8, D-85748 Garching, Germany*

<sup>2</sup> *L. D. Landau Institute for Theoretical Physics, 142432 Chernogolovka, Russia*

<sup>3</sup> *European Synchrotron Radiation Facility, F-38043 Grenoble, France*

(Dated: 22nd March 2022)

## Abstract

A superposition of the Pauli and orbital coupling of a high magnetic field to charge carriers in a charge-density-wave (CDW) system is proposed to give rise to transitions between subphases with quantized values of the CDW wavevector. By contrast to the purely orbital field-induced density-wave effects which require a strongly imperfect nesting of the Fermi surface, the new transitions can occur even if the Fermi surface is well nested at zero field. We suggest that such transitions are observed in the organic metal  $\alpha$ -(BEDT-TTF)<sub>2</sub>KHg(SCN)<sub>4</sub> under a strongly tilted magnetic field.

A quantization of the orbital motion of charge carriers in quasi-one-dimensional (Q1D) organic conductors (TMTSF)<sub>2</sub>X under high magnetic fields leads to a remarkable quantum phenomenon of field-induced spin-density waves (FISDW) (see [1, 2] for a review). In these salts, the conducting band can be described near the Fermi level by the simplified dispersion law:

$$\epsilon(\mathbf{k}) = \hbar v_F (|k_x| - k_F) - 2t_y \cos(k_y a_y) - 2t'_y \cos(2k_y a_y) - 2t_z \cos(k_z a_z), \quad (1)$$

where  $\frac{t_y}{E_F} \sim \frac{t'_y}{t_y} \simeq 0.03$ ;  $\frac{t_z}{E_F} \sim 10^{-3}$ ;  $E_F$ ,  $v_F$ , and  $k_F$  are, respectively, the Fermi energy, Fermi velocity and Fermi wavenumber in the chain direction  $x$ ;  $a_y$  and  $a_z$  are the interchain distances. Correspondingly, the Fermi surface (FS) is represented by two flat, only slightly warped sheets extended in  $k_y k_z$  plane. At small  $t'_y$  such a FS is subject to a nesting instability resulting in an insulating charge-density wave (CDW) or spin-density wave (SDW) groundstate [1]. In the (TMTSF)<sub>2</sub>X salts the groundstate is a SDW. One can increase the “antinesting” term  $t'_y$ , e.g. by applying pressure, thereby weakening the nesting instability. At  $t'_y > t'^*_y \simeq k_B T_c(0)$  [where  $T_c(0)$  is the density-wave transition temperature at  $t'_y = 0$ ] the SDW is completely suppressed [3, 4, 5]. However, a magnetic field  $\mathbf{B}$  applied along the  $z$ -axis restricts electron orbits to the chain direction, i.e. enhances their one-dimensionality, and restores the SDW state [2, 5, 6, 7]. Since the FS nesting is strongly imperfect, the new SDW state is semimetallic rather than insulating. Under a high magnetic field the semimetallic spectrum is subdivided into Landau subbands and the system gains energy when the Fermi level is situated between adjacent subbands. This can be achieved by an appropriate choice of the nesting vector  $\mathbf{Q}$  which determines the size of the semimetallic pockets. As a result,  $\mathbf{Q}$  becomes field-dependent, deviating from its ideal value  $\mathbf{Q}_0 = (2k_F, \pi/a_y, \pi/a_z)$ , and at low enough temperatures the system undergoes a series of first order phase transitions to FISDW subphases with quantized values of the  $Q_x$  component [1, 2, 7, 8, 9, 10]:

$$Q_{xN} = 2k_F + NG, \quad (2)$$

where  $N$  is an integer and  $G = 2ea_y B_z / \hbar c$ .

Similarly, the orbital effect has been predicted to produce field-induced charge-density wave (FICDW) subphases [11, 12]. The theoretical predictions are supported by recent pressure-dependent magnetotransport studies of the organic conductor  $\alpha$ -(BEDT-TTF)<sub>2</sub>KHg(SCN)<sub>4</sub> [13] which is believed to be in a CDW state with a nested Q1D part

of its FS below  $\simeq 8.5$  K [14, 15, 16, 17]. However, in comparison with the SDW case, the situation in CDW systems is more complicated due to the presence of an additional, Pauli effect. The CDW formation is based on the pairing interaction between the electrons and holes having the same spin and separated in  $k$ -space by a unique wavevector (nesting vector)  $\mathbf{Q}$ . A magnetic field lifts the degeneracy between two subbands with the parallel and antiparallel spins, respectively, so that the zero-field wavevector does not provide optimal nesting conditions for either of the subbands. This leads to a decrease of the critical temperature  $T_c(B)$  [18]. It is mainly the Pauli effect which determines the shape of the  $B-T$  phase diagram of  $\alpha$ -(BEDT-TTF) $_2$ KHg(SCN) $_4$  at ambient pressure, in the field perpendicular to the highly conducting  $ac$ -plane [15, 16]. However, the orbital effect was also suggested to play a significant role under pressure [13] or in a magnetic field strongly tilted towards the  $ac$ -plane [19].

In this Letter, we propose that the superposition of Pauli and orbital effects of a high magnetic field on a CDW can give rise to a series of transitions between subphases with quantized values of the nesting vector. By contrast to the above mentioned FISDW and FICDW effects, these new transitions do not require a suppressed density wave state at zero magnetic field ( $t'_y > t_y^*$ ). We analyze the complex behavior of  $\alpha$ -(BEDT-TTF) $_2$ KHg(SCN) $_4$  in tilted magnetic fields and argue that the proposed phenomenon is realized in this compound.

The field-induced transitions in single crystals of  $\alpha$ -(BEDT-TTF) $_2$ KHg(SCN) $_4$  were studied by simultaneous measurements of magnetic torque and resistivity versus magnetic field as described elsewhere [20]. The resistivity was measured in the  $b^*$  direction ( $b^* \perp ac$ ). The sample could be turned with respect to the magnetic field and its orientation was defined by the tilt angle  $\theta$  between the  $b^*$ -axis and the field direction. The absolute value of  $\theta$  was determined to the accuracy of  $\leq 0.1^\circ$ . This was assured by measuring the frequency of the de Haas-van Alphen (dHvA) oscillations originating from the second, quasi-two-dimensional, conducting band which precisely follows the  $1/\cos\theta$ -law.

We start with a qualitative consideration of the field dependence of the  $x$  component of the nesting vector for a CDW system described by the dispersion relation (1) with a negligibly small  $t_z$  and  $0 < t'_y < t_y^*$ . Treating each spin subband independently, one can express the optimal nesting conditions as  $Q_{\text{opt},x}^{\uparrow(\downarrow)}(B) = Q_{0x} \pm 2\mu_B B / \hbar v_F$ , where the sign  $+$ ( $-$ ) stands for the spins parallel (antiparallel) to the applied field (see dashed lines in Fig.1).

Nevertheless, the system as a whole maintains the constant nesting vector  $\mathbf{Q}_0$  and both subbands will remain fully gapped up to the critical field  $B_k \sim \Delta_{\text{CDW}}/2\mu_B$ , where  $\Delta_{\text{CDW}}$  is the CDW energy gap [11]. Above  $B_k$ ,  $\mathbf{Q}_0$  is no more a good nesting vector as it leads to ungapped states in both subbands. Then, at low enough temperatures,  $T < T^* \simeq 0.6T_c(0)$ , a  $\text{CDW}_x$  state with the field-dependent nesting vector,  $Q_x(B) = Q_{0x} + q_x^{\text{Pauli}}(B)$ , is formed [11, 21]. The additional term  $q_x^{\text{Pauli}}(B)$  asymptotically approaching the value  $2\mu_B B/\hbar v_F$  is schematically shown in Fig. 1 by the thin solid line. With this term the nesting conditions are obviously improved for one of the spin subbands (say, the spin-up subband) at the cost of an additional unnesting of the other (spin-down).

So far the Pauli effect was considered as a mechanism dominating the evolution of the CDW in a magnetic field. If the antinesting term  $t'_y$  is sufficiently lower than the critical value  $t_y^*$ , the orbital effect below  $B_k$  only leads to a small increase of the CDW gap with increasing field. However, for  $B > B_k$  one should take into account that the carriers of the spin-down subband become partially ungapped. If the field is not too high, this subband forms small, closed in  $k_x k_y$  plane pockets [22]. The situation resembles the “conventional” FISDW or FICDW cases with  $t'_y \gtrsim t_y^*$ ; only the unnesting role is taken by the Pauli effect. Therefore, one can expect the orbital quantization condition in the form of Eq.(2) to be set on the nesting vector. However, the quantized levels should be now counted from  $Q_{\text{opt},x}^\downarrow(B)$ :

$$Q_{x,N}^{\text{orbit}} = Q_{0x} - 2\mu_B B/\hbar v_F + NG. \quad (3)$$

The corresponding values  $q_{x,N}^{\text{orbit}} = Q_{x,N}^{\text{orbit}} - Q_{0x}$  are schematically shown by dotted lines in Fig. 1.

As a result, the most favorable values of the nesting vector above  $B_k$  are determined by intersections of the continuous curve  $q_x^{\text{Pauli}}(B)$  with the straight lines  $q_{xN}^{\text{orbit}}$ , i.e. by the superposition of the Pauli and quantum orbital effects. Thus, with changing the field we obtain a series of first order transitions between CDW subphases characterized by different quantized values of the nesting vector as schematically shown by thick lines in Fig. 1. Note that our model implies an increase of the quantum number  $N$  with increasing  $B$ , in contrast to what is usually observed in known orbital quantization phenomena.

The presented qualitative model will now be compared with the experimental results on  $\alpha\text{-(BEDT-TTF)}_2\text{KHg(SCN)}_4$ . Fig. 2 shows magnetic torque and interlayer resistance recorded at increasing (solid lines) and decreasing (dashed lines) field sweeps, at  $\theta = 81.4^\circ$ . In

agreement with previous reports [16, 19, 23], below 2 K both quantities consistently display irregular oscillations with a significant hysteresis. Both the amplitude of the oscillations and strength of the hysteresis rapidly increase with decreasing temperature. The so-called kink transition at  $B_k \approx 12.7$  T is supposed to be the transition between the  $\text{CDW}_0$  groundstate and  $\text{CDW}_x$  [13, 14, 15, 16]. This transition is considerably shifted from its zero-angle value  $B_k(\theta = 0) \approx 24$  T (see inset in Fig. 2 for comparison). In addition, there are two features at higher fields reminiscent of first order phase transitions.

In order to clarify the origin of the observed structure, we have studied in detail how it develops with changing  $\theta$ . In the following we analyze the torque data divided by  $\sin(2\theta)$  in order to enable a direct comparison between the curves recorded at different  $\theta$ 's. The features in the magnetoresistance are found to correlate with those in the torque (see e.g. Fig. 2) although at  $\theta$  approaching  $90^\circ$  they become more smeared and difficult to interpret in terms of phase transitions.

Fig. 3 shows the field-dependent torque at different angles,  $T = 0.4$  K (the curves are vertically shifted with respect to each other for clarity). The data represented by solid lines have been taken at increasing  $B$ ; additionally, down sweeps are shown for  $81^\circ < \theta < 84^\circ$  (dashed lines) to illustrate the hysteresis. The curves corresponding to  $\theta < 81^\circ$  have been obtained by filtering out the dHvA oscillations from the measured signal. An example of the total signal, including the oscillations, at  $\theta = 67.1^\circ$  is given by the grey dotted line in Fig. 3a.

At relatively low angles, one can see a sharp kink transition which takes place at  $\approx 22.5$  T at  $53^\circ$ . It gradually shifts down, saturating at  $\simeq 10$  T as  $\theta$  approaches  $90^\circ$ . As  $B_k$  decreases below 20 T, the transition becomes less pronounced although can still be detected up to  $\theta \approx 85^\circ$ . Below  $B_k$ , a weak additional feature is observed up to  $78^\circ$  (dotted line in Fig. 3a). While its origin is not clear at present, it may be related to the hysteretic changes of the magnetoresistance [24, 25] and magnetothermopower [26] observed in the same field range earlier.

Starting from  $65^\circ$ , new features emerge at the high-field side, moving to lower fields with further increasing  $\theta$ . Like the kink transition, they are rather sharp at high fields and gradually fade below 20 T. The structure changes with increasing rate at  $\theta \rightarrow 90^\circ$ . At the same time the features become less pronounced and could not be resolved above  $88^\circ$ . While the observed behavior is strongly suggestive of multiple phase transitions, at the moment it

is difficult to determine the exact location of each transition. However, taking into account the character of changes in the magnetization and the hysteresis behavior, it is reasonable, by analogy with  $B_k$ , to identify the transition points with local maxima in the derivative  $(\partial M/\partial B)_\theta$ .

Such points are plotted in Fig. 4 in the form of a  $B - \theta$  phase diagram. In the inset the same data are replotted against  $1/\cos\theta$  in order to show the region near  $90^\circ$  in more detail. The crosses represent  $B_k(\theta)$ , the empty circles correspond to the weak feature below  $B_k$ , and the solid circles delineate the boundaries between new subphases within the high-field state. There is a clear tendency for all the transitions to shift to lower fields with increasing  $\theta$ . Further, the increasingly strong angular dependence in the vicinity of  $\theta = 90^\circ$  and the absence of the features at the exactly parallel orientation suggest that the orbital effect determined by the perpendicular component of magnetic field  $B_z = B \cos \theta$  plays a crucial role. On the other hand, the CDW state is obviously subject to the strong Pauli effect at  $B > B_k$  [11]. Therefore it is very likely that the observed transitions originate from an interplay between the Pauli and orbital effects on the high field CDW state.

From Fig. 1 it is clear that the proposed multiple transitions can only take place if more than one quantum level intersect the  $q_x^{\text{Pauli}}(B)$  curve, i.e. when  $3G = 6ea_y B_z/\hbar c < 4\mu_B B/\hbar v_F$ . This condition is obviously not satisfied at low  $\theta$  where only one, kink transition is observed. With increasing  $\theta$ , the separation between the levels,  $G$ , proportional to the perpendicular field component  $B_z$  decreases whereas the isotropic Pauli effect remains unchanged. Starting from a threshold angle  $\theta^*$ , the above condition becomes fulfilled and a new transition emerges at a high field, shifting towards  $B_k$  at a further increase of  $\theta$ . In our experiment the first transition above  $B_k$  is found at  $\theta \approx 65^\circ$ . This allows us to estimate the upper limit for the Fermi velocity in the 1D direction:  $v_F \lesssim 2\mu_B c/3ea_y \cos 65^\circ \approx 9 \times 10^6$  cm/sec, which is in good agreement with the recently reported value  $v_F = 6.5 \times 10^6$  cm/sec [27]. Thus, the proposed model explains not only the occurrence of multiple first-order transitions above  $B_k$ , but also the threshold angle above which they start to appear as well as the general tendency of them to shift towards  $B_k$  with further tilting the field.

Obviously, the sharpness of the transitions between the quantum orbital levels should strongly depend on temperature and on the strength of the perpendicular field component. This is consistent with the observed damping of the structure with increasing temperature (Fig. 2) or at  $\theta$  very close to  $90^\circ$  (Fig. 3b).

The experimental phase diagram (Fig. 4) looks more complicated than it would be expected within the present qualitative model: some phase lines appear to be split, giving rise to additional subphases. This disagreement is, however, not surprising. On the one hand, it is not excluded that the additional phase,  $\text{CDW}_y$  ( $q_x = 0; q_y \neq 0$ ), which was not taken into account here, emerges at a certain angular and field range [11, 19]. On the other hand, the orbital quantization effects are known to strongly depend on the exact FS geometry, i.e on details of the antinesting term, in the case of FISDW [28]. According to the band structure calculations [29], the antinesting term in the present compound must be significantly more complex than suggested by the model spectrum (1). Therefore it is expected to also lead to considerable complications in high-field subphase structure. There are other open questions, such as the transition-like feature below  $B_k$  and the considerable (although at a slower rate) decrease of  $B_k$  with increasing  $\theta$ . A development of a quantitative theory will certainly help to understand the entire phase diagram of the present compound and to get a deeper insight into the interplay of the Pauli and orbital effects on CDW.

The experimental data presented in this paper have been obtained at the Grenoble High Magnetic Field Laboratory. The work was supported by HPP Programme of EU, contracts HPRI-1999-CT-00030 and HPRI-CT-1999-40013, INTAS grant 01-0791, and RFBR 03-02-16121.

- 
- [1] T. Ishiguro, K. Yamaji, and G. Saito, *Organic Superconductors*, 2<sup>nd</sup> edition (Springer-Verlag Berlin Heidelberg, 1998).
  - [2] P. M. Chaikin, J. Phys. I France **6**, 1875 (1996).
  - [3] G. M. Danner, P. M. Chaikin, and S. T. Hannahs, Phys. Rev. B **53**, 2727 (1996).
  - [4] K. Yamaji, J. Phys. Soc. Jpn. **51**, 2787 (1982); Y. Hasegawa and H. Fukuyama, J. Phys. Soc. Jpn. **55**, 3978 (1986).
  - [5] G. Montambaux, Phys. Rev. B **38**, 4788 (1988).
  - [6] J. F. Kwak et al., Phys. Rev. Lett. **56**, 972 (1986).
  - [7] L. P. Gor'kov and A. G. Lebed, J. Phys. (Paris) Lett. **45**, L433 (1984).
  - [8] G. Montambaux, M. Héritier, and P. Lederer, Phys. Rev. Lett. **55**, 2078 (1985).
  - [9] A. G. Lebed, Phys. Rev. Lett. **88**, 177001 (2002); A. G. Lebed, Pis'ma Zh. Teor. Eksp. Fiz. **72**, 205 (2000) [JETP Lett. **72**, 141 (2000)].
  - [10] K. Sengupta and N. Dupuis, cond-mat/0302142, unpublished.
  - [11] D. Zanchi, A. Bjeliš, and G. Montambaux, Phys. Rev. B **53**, 1240 (1996).
  - [12] A. G. Lebed, Synth. Metals in press.
  - [13] D. Andres et al., Phys. Rev. B **64**, 161104(R) (2001).
  - [14] R. H. McKenzie, cond-mat/9706235, unpublished.
  - [15] N. Biskup, J. A. A. J. Perenboom, J. S. Qualls, and J. S. Brooks, Solid State Commun. **107**, 503 (1998).
  - [16] P. Christ et al., JETP Lett. **71**, 303 (2000).
  - [17] P. Foury-Leylekian, S. Ravy, J. P. Pouget, and H. Müller, Synth. Met., to be published.
  - [18] W. Dieterich and P. Fulde, Z. Physik **265**, 239 (1973).
  - [19] J. S. Qualls et al., Phys. Rev. B **62**, 10008 (2000).
  - [20] H. Weiss et al., Phys. Rev. B **60**, R16259 (1999).
  - [21] We do not consider here an additional, CDW<sub>y</sub> state with a field-dependent  $y$  component of the nesting vector which was suggested to exist in a narrow field range for certain values of electron coupling constants [11]. This, however, does not affect the physical nature of the described phenomenon.
  - [22] Based on geometrical considerations, one can roughly estimate the upper limit for the field,



- at which closed pockets are formed, from the condition:  $2\mu_B B + \hbar q_x^{\text{Pauli}} v_F - \Delta_{\text{CDW}} < 2t'_y$ .
- [23] P. Christ et al., *Synth. Metals* **70**, 823 (1996).
  - [24] N. Harrison et al., *Phys. Rev. B* **55**, R16005 (1997).
  - [25] C. Proust et al., *Phys. Rev. B* **62**, 2388 (2000).
  - [26] E. S. Choi, J. S. Brooks, and J. S. Qualls, *Phys. Rev. B* **65**, 205119 (2002).
  - [27] A. E. Kovalev, S. Hill, and J. S. Qualls, *Phys. Rev. B* **66**, 134513 (2002).
  - [28] D. Zanchi and G. Montambaux, *Phys. Rev. Lett.* **77**, 366 (1996).
  - [29] R. Rousseau et al., *J. Phys. I France* **6**, 1527 (1996); M. Gusmão and T. Ziman, *Phys. Rev. B* **54**, 16663 (1996).

## Figure captions

Fig. 1. Schematic illustration of the field dependence of the CDW wavevector (thick line) originating from the superposition of the Pauli effect (thin solid line) [11] and orbital quantization. The quantized orbital levels (dotted lines) are counted from  $q_{\text{opt},x}^{\downarrow}(B)$  corresponding to the optimal nesting vector for the spin-down subband which is partially ungapped above  $B_k$ .

Fig. 2. (a) Up (solid lines) and down (dashed lines) field sweeps of the magnetic torque of  $\alpha$ -(BEDT-TTF)<sub>2</sub>KHg(SCN)<sub>4</sub> at  $\theta = 81.4^\circ$ , at  $T = 0.4$  and  $1.3$  K. (b) The same for the inter-layer resistance. Vertical line indicates the kink transition field  $B_k$ . Inset: magnetoresistance at a low  $\theta$ ,  $T = 0.4$  K.

Fig. 3. Evolution of the high-field structure in the steady torque with changing  $\theta$ . Solid lines: up sweeps of the field; dashed lines (at  $81^\circ < \theta < 84^\circ$ ): down sweeps. For  $\theta < 81^\circ$  the dHvA signal is subtracted; an example of the total signal is given by the grey dotted line for  $\theta = 67.1^\circ$ .

Fig. 4.  $B - \theta$  phase diagram of  $\alpha$ -(BEDT-TTF)<sub>2</sub>KHg(SCN)<sub>4</sub>. Crosses: kink transition  $B_k$ ; open circles: weak feature below  $B_k$ ; solid circles: multiple transitions inside the high-field state. Lines are guides to the eye.

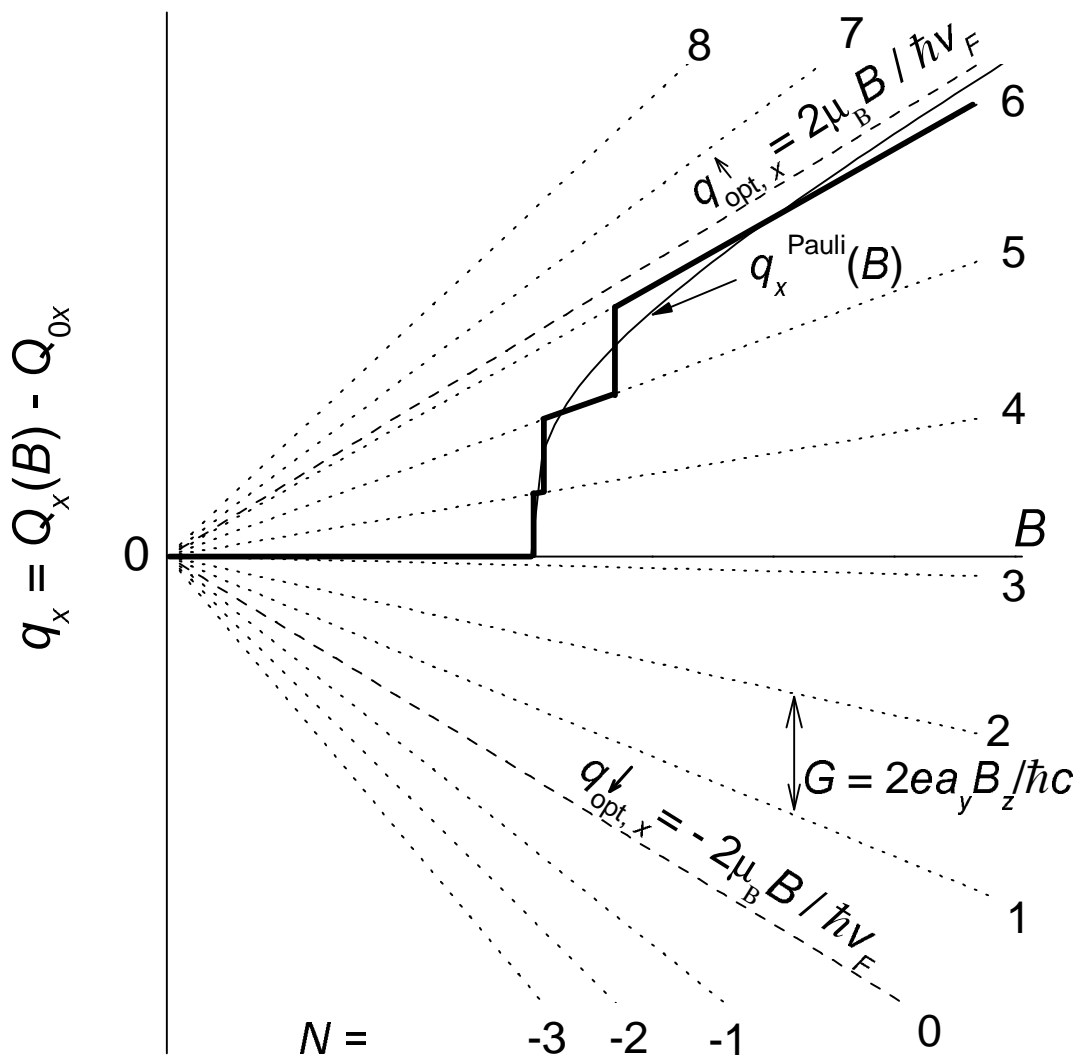


Fig. 1 of "Orbital quantization..." by D. Andres et al.

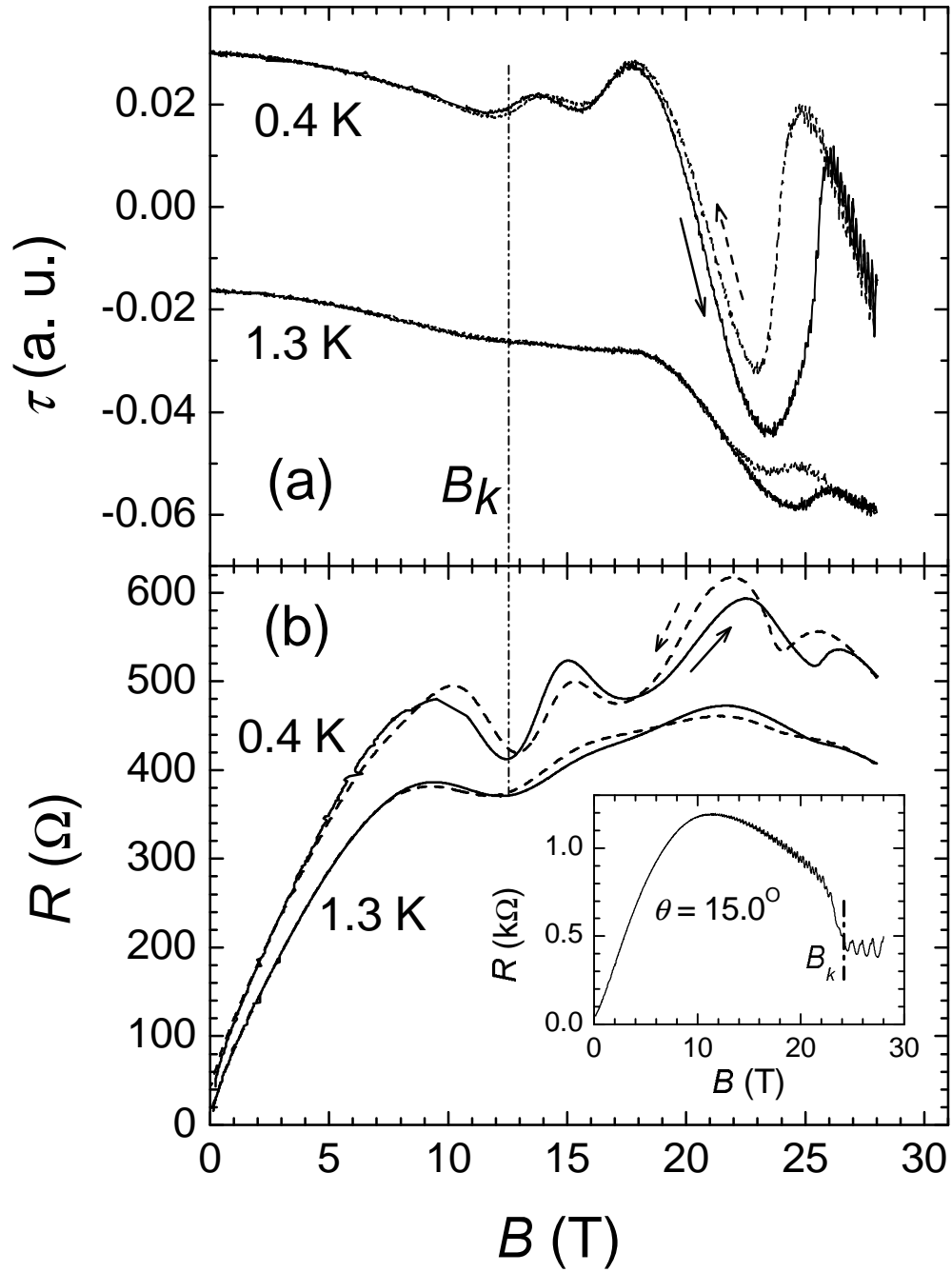


Fig. 2 of "Orbital quantization..." by D. Andres et al.

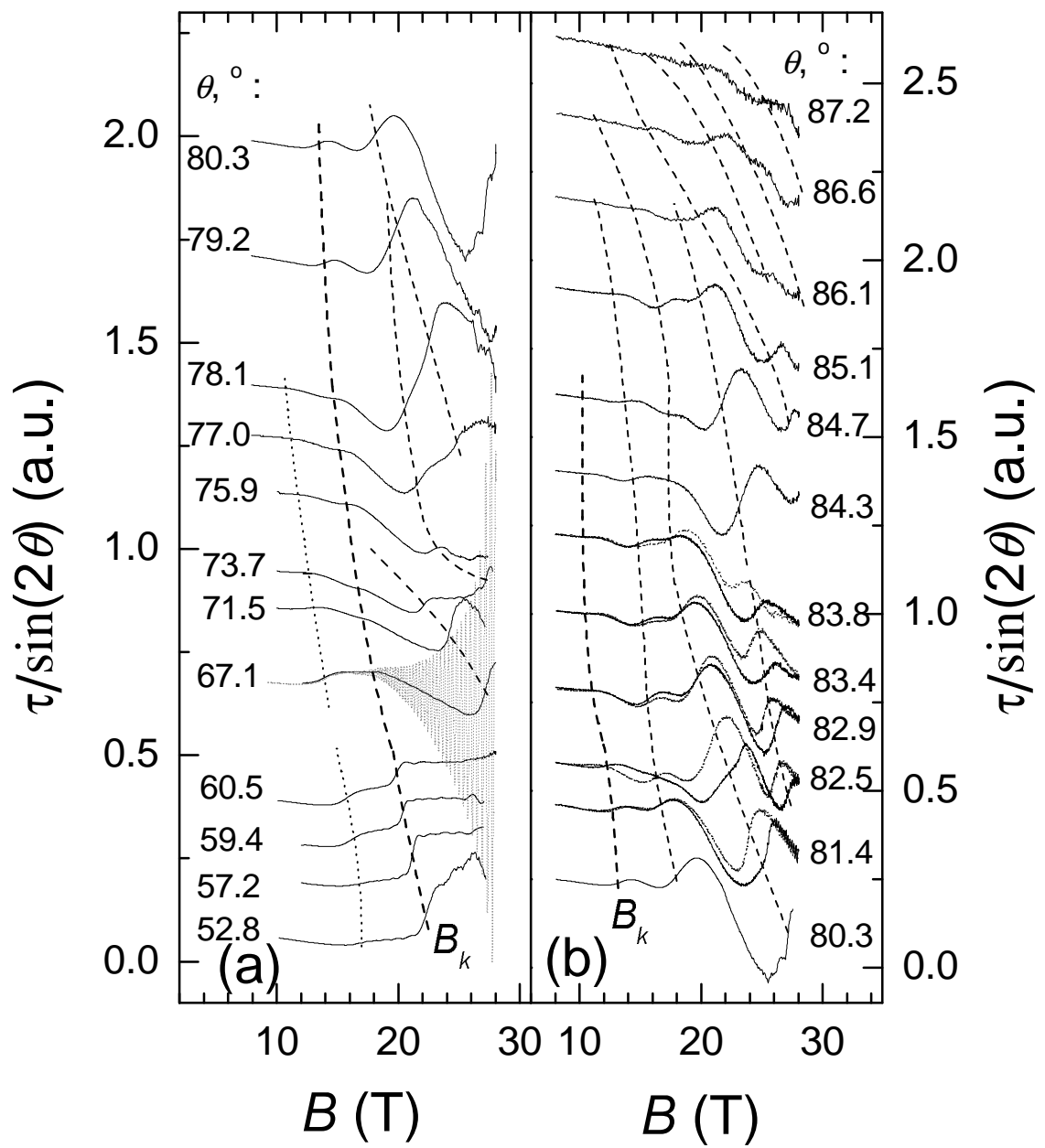


Fig. 3 of "Orbital quantization..." by D. Andres et al.

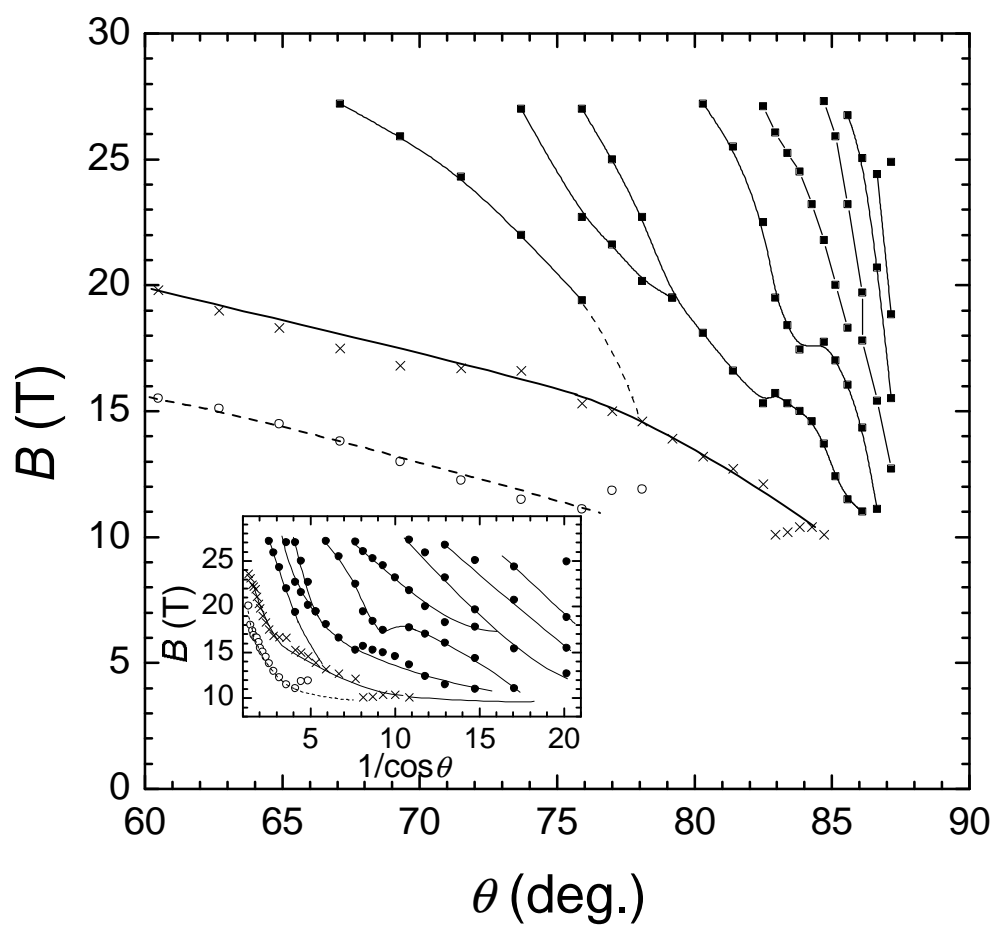


Fig. 4 of "Orbital quantization..." by D. Andres et al.